Research Square

Preprints are preliminary reports that have not undergone peer review.
They should not be considered conclusive, used to inform clinical practice,
or referenced by the media as validated information.

Allelic heterogeneity and cystic pathway modulation in HNF1B disease

Caroline M. Kolvenbach
Harvard Medical School
Ken Saida
Harvard Medical School
Elena Zion
Harvard Medical School
Selina Hölzel
Harvard Medical School
Izzeldin Elmubarak
Harvard Medical School
Gina Kalkar
Harvard Medical School
Katharina Lemberg
Harvard Medical School
Shirlee Shril
Harvard Medical School
Friedhelm Hildebrandt
friedhelm.hildebrandt@childrens.harvard.edu

Harvard Medical School

Article

Keywords: HNF1B, CAKUT, cystic kidney disease, genotype-phenotype correlation, drug repurposing

Posted Date: November 12th, 2026

DOI: https://doi.org/10.21203/rs.3.rs-11277319/v1

License: This work is licensed under a Creative Commons Attribution 4.0 International License.
Read Full License

Additional Declarations: No competing interests reported.

Allelic heterogeneity and cystic pathway modulation in *HNF1B* disease

Authors

Caroline M. Kolvenbach[1,2], Ken Saida[1], Elena Zion[1], Selina Hölzel[1], Izzeldin Elmubarak[1], Gina Kalkar[1], Katharina Lemberg[1,3], Shirlee Shril[1], Friedhelm Hildebrandt[1,*]

Affiliations

1 Department of Pediatrics, Boston Children's Hospital, Harvard Medical School, Boston, Massachusetts, USA.

2 Department of Pediatrics I, University Children's Hospital Heidelberg, Medical Faculty, Heidelberg University, Heidelberg, Germany.

3 Department II of Internal Medicine and Center for Molecular Medicine Cologne, University of Cologne and University Hospital Cologne, Cologne, Germany.

*Corresponding author

Correspondence

Friedhelm Hildebrandt, M.D.

Division of Nephrology, Boston Children's Hospital

300 Longwood Avenue

Boston, Massachusetts 02115

friedhelm.hildebrandt@childrens.harvard.edu

+1 617 355-6129

ABSTRACT (171/200 words)

Heterozygous *HNF1B* variants cause a clinically heterogeneous disorder ranging from isolated renal anomalies to renal cysts and diabetes (RCAD) syndrome. To define allele-level genotype–phenotype relationships, we curated 329 pathogenic or likely pathogenic intragenic *HNF1B* variants from ClinVar and HGMD and annotated reported RCAD, kidney-only and diabetes-only phenotypes. Predicted loss-of-function (pLOF) variants were more frequently associated with RCAD, whereas missense variants were enriched for diabetes-only presentations. Missense variants showed substantial phenotypic overlap without clear domain-specific segregation. Higher AlphaMissense scores were observed among RCAD-associated missense variants, although DNA-binding-domain localization showed the stronger association with RCAD. To test whether cystogenesis resulting from *Hnf1b* loss remains pharmacologically modifiable, we evaluated selected cystogenic pathways and glutamatergic signaling in a kidney-specific *Hnf1b* knockout mouse model. CFTR inhibition, vasopressin receptor antagonism and systemic AMPK activation reduced cystic burden, whereas NMDA receptor modulation showed no significant effect. These findings support partial variant-class-associated phenotypic effects in *HNF1B* disease while highlighting extensive allele-level pleiotropy, and provide *in vivo* proof-of-concept that selected downstream cystogenic pathways remain pharmacologically modifiable despite *Hnf1b* loss.

KEYWORDS

HNF1B, CAKUT, cystic kidney disease, genotype-phenotype correlation, drug repurposing

INTRODUCTION

Heterozygous variants in the transcription factor *HNF1B* (hepatocyte nuclear factor 1β) are among the most common monogenic causes of developmental kidney disease and produce a multisystem disorder termed *HNF1B*-associated disease[1–4]. Renal manifestations include cysts, dysplasia, hyperechogenic parenchyma and congenital anomalies of the kidney and urinary tract (CAKUT), frequently progressing to chronic kidney disease, while extrarenal features range from MODY5 diabetes to pancreatic atrophy, hypomagnesemia and genital malformations[1–4]. More than 50% of affected individuals ultimately develop chronic kidney disease, and a substantial proportion progress to end-stage kidney disease. Despite this considerable clinical burden, treatment remains supportive only and no disease-modifying therapies currently exist.

A defining feature of *HNF1B*-associated disease is its marked phenotypic heterogeneity and variable expressivity. Clinical manifestations vary widely not only between unrelated individuals but also among carriers of identical variants, even within the same family, suggesting mechanisms beyond uniform haploinsufficiency[1]. While whole-gene deletions account for approximately 50% of *HNF1B*-associated disease, intragenic *HNF1B* variants comprise a broad spectrum of pLOF and missense alleles with incompletely understood genotype-phenotype relationships[2,3]. Emerging evidence suggests that genotype may influence clinical expression. In particular, individuals with intragenic *HNF1B* variants exhibit poorer kidney survival than individuals with 17q12 deletions, and variants affecting the POU-specific DNA-binding domain have been associated with more severe kidney disease[5]. More recently, a patient-level systematic review reported that truncating *HNF1B*

variants were associated with a higher prevalence of renal manifestations and a lower prevalence of diabetes than non-truncating variants, while variants within the DNA-binding domain were associated with more severe renal and extrarenal phenotypes[6]. Together, these observations support partial genotype–phenotype associations in *HNF1B*-associated disease. However, whether individual intragenic *HNF1B* alleles show reproducible differences in their reported phenotypic spectrum, and to what extent such patterns reflect variant class or protein-domain localization, remains unclear.

At the molecular level, HNF1B functions as a central regulator of epithelial differentiation, tubular morphogenesis and transcriptional programs implicated in cystic kidney disease, including *PKD2*- and *PKHD1*-associated pathways[7,8]. *HNF1B* has also been implicated as a modifier of *PKD1*-associated disease, suggesting mechanistic convergence with ADPKD[9]. These observations provide a rationale to evaluate whether pharmacologic approaches targeting ADPKD-associated signaling pathways may also attenuate cystogenesis in *HNF1B*-associated disease[10–13]. In parallel, transcriptomic analyses of HNF1B-deficient epithelia identified alterations in glutamatergic signaling-related genes, suggesting a potential contribution of glutamatergic pathways to *HNF1B*-associated epithelial dysfunction[14].

Here, we systematically curated disease-associated intragenic *HNF1B* variants to characterize allele-level phenotypic heterogeneity across variant classes and protein domains. In parallel, we evaluated whether cystogenesis caused by *Hnf1b* loss remains

susceptible to pharmacologic modulation of established cystogenic and glutamatergic pathways in a kidney-specific *Hnf1b* knockout (KO) mouse model.

RESULTS

We curated 329 intragenic *HNF1B* variants meeting the predefined inclusion criteria (**Methods**). The final cohort comprised 203 pLOF and 126 missense variants (**Fig. 1**). Phenotypes were categorized as RCAD, kidney-only or diabetes-only presentations. Phenotypic annotations were curated at the allele level, allowing individual variants to be associated with multiple reported clinical presentations.

Stratification by variant class revealed significant differences in phenotypic distribution (**Fig. 2A–B**). RCAD phenotypes were observed in 77.3% of pLOF variants compared with 65.1% of missense variants (157/203 vs. 82/126; P=0.022), whereas diabetes-only presentations were significantly more frequent among missense variants (53.2% vs. 37.9%; 67/126 vs. 77/203; P=0.0085). In contrast, kidney-only phenotypes did not differ significantly between variant classes (40.5% vs. 42.4%; 51/126 vs. 86/203; P=0.82). A sensitivity analysis excluding eight alleles for which RCAD classification was based solely on nonspecific *HNF1B*-related disease annotations yielded comparable results, with RCAD reported for 76.8% of pLOF and 64.2% of missense alleles (152/198 vs. 79/123; P=0.021). Analysis of phenotype combinations demonstrated substantial overlap between RCAD, kidney-only and diabetes-only presentations across individual alleles, highlighting marked phenotypic pleiotropy (**Fig. 2C**).

To further assess potential allele-specific effects, 126 missense variants were mapped across the HNF1B protein domains (**Fig. 3A**). Variants associated with RCAD, kidney-only and diabetes-only phenotypes were distributed throughout the protein without

evident clustering within specific functional domains. A modest trend toward enrichment of RCAD-associated variants within the DNA-binding domains and diabetes-associated variants within the transactivation domain was observed; however, χ^2 residual analysis did not identify strong domain-specific segregation overall (all standardized residuals < |2|; **Fig. S1A**).

AlphaMissense analysis provided further evidence for differences among missense alleles. RCAD-associated variants showed higher predicted deleteriousness than variants without an RCAD annotation (median score 0.996 versus 0.878; Holm-adjusted P=0.026), whereas no significant differences were observed for kidney-only or diabetes-only phenotypes (both adjusted P=1.000; **Fig. 3B**). However, this association was not observed when variants were stratified by localization within or outside the DNA-binding domains. In logistic regression, DNA-binding-domain localization remained associated with RCAD (OR 3.39, 95% CI 1.22–9.45; P=0.019), whereas AlphaMissense score was not independently associated with RCAD (OR 1.94, 95% CI 0.43–8.67; P=0.386; **Fig. S1B**).

Because human *HNF1B* disease exhibits marked allelic heterogeneity and variable expressivity without strict domain segregation, we next asked whether cystogenesis caused by *Hnf1b* loss might nevertheless converge on pharmacologically tractable downstream pathways. We therefore tested candidate compounds targeting pathways implicated in cystic kidney disease or glutamatergic signaling in an *Hnf1b* KO mouse model[7–9]. Candidate compounds were selected based on efficacy in ADPKD models or relevance to glutamatergic signaling and included the CFTR inhibitor CFTRinh172, the

vasopressin V2 receptor antagonist conivaptan, the AMPK activator metformin, the SMYD2 inhibitor AZ505, and modulators of NMDA receptor signaling (NMDA and MK-801; **Fig. 4; Fig. S2)**[10–14].

Histological and morphometric analyses demonstrated that three ADPKD-directed compounds - CFTRinh172, conivaptan and metformin administered in drinking water - were associated with a statistically significant reduction in cystic index relative to untreated KO controls (**Fig. 5A**). The corresponding mean differences versus untreated KO controls were −4.14 (95% CI −6.78 to −1.49), −3.48 (95% CI −5.59 to −1.36), and −5.18 (95% CI −7.57 to −2.80), respectively. These findings suggest that inhibition of CFTR-mediated fluid secretion, suppression of vasopressin signaling and activation of AMPK-associated pathways may attenuate early cyst growth in *HNF1B*-associated disease.

In contrast, AZ505, an inhibitor of the lysine methyltransferase SMYD2, did not significantly alter cystic burden (**Fig. 5A**). Likewise, modulation of glutamatergic signaling using either NMDA or the NMDAR antagonist MK-801 failed to improve cystogenesis. Although MK-801-treated animals showed a trend toward increased cyst formation, this did not reach statistical significance (**Fig. 5A**).

The 2-kidneys-to-body-weight ratio (2KW/BW) was evaluated as an additional marker of disease severity. A significant increase in 2KW/BW was observed only in CFTRinh172-treated animals (**Fig. 5B**). However, this effect appeared attributable to reduced overall

body weight rather than increased kidney mass, as absolute kidney weights were not significantly increased.

To determine whether structural improvements translated into functional benefit, serum creatinine and blood urea nitrogen (BUN) levels were assessed at the examined early timepoint. Across all treatment groups, including those demonstrating reduced cystic burden, no significant improvement in renal retention parameters was observed compared with untreated KO mice (**Fig. 5C–D**). Representative histological sections confirmed reduced cyst area following CFTR inhibition (**Fig. 5E**).

DISCUSSION

Our data demonstrate substantial allelic and phenotypic heterogeneity in *HNF1B*-associated disease. While pLOF variants were more frequently associated with RCAD phenotypes, missense variants showed significant enrichment for diabetes-only presentations. These findings are consistent with a recent patient-level systematic review reporting more frequent renal manifestations and less frequent diabetes in individuals carrying truncating *HNF1B* variants[6]. Thus, patient-level data independently support the direction of the variant-class associations observed in our allele-level analysis, while our approach additionally reveals substantial phenotypic pleiotropy across individual recurrent alleles. The relative enrichment of diabetes-only phenotypes among missense alleles suggests that not all *HNF1B* variants exert equivalent biological effects. One possible explanation is that some missense variants retain partial or tissue-dependent transcriptional activity. However, the extensive overlap of RCAD, kidney-only and diabetes-only presentations among individual alleles indicates that variant class alone does not determine clinical expression.

Consistent with this complexity, missense variants showed no strong overall segregation of reported phenotypes across HNF1B protein domains. HNF1B functions within complex transcriptional and ciliopathy-associated regulatory networks, raising the possibility that modifier genes, stochastic developmental effects, or differences in compensatory signaling pathways influence phenotypic expression. The particularly broad renal phenotypic spectrum associated with *HNF1B* disease may therefore reflect both

developmental dosage sensitivity and context-dependent buffering mechanisms within distinct epithelial compartments.

Several limitations should be considered when interpreting the human genetic analyses. Phenotypic annotations were curated from ClinVar and HGMD entries and therefore depended on the level of clinical detail provided in the original reports. In some cases, variants may have been classified as RCAD despite only partial phenotypic information being available, whereas additional renal or diabetic manifestations may not have been systematically reported. Conversely, variants annotated as kidney-only or diabetes-only may have reflected incomplete phenotyping rather than truly isolated disease manifestations. Such inconsistencies in phenotype annotation could contribute to imprecision in genotype-phenotype correlations and potentially obscure subtle domain- or allele-specific effects. Because the analysis was performed at the allele rather than patient level, the observed proportions do not represent penetrance or phenotype frequencies among variant carriers.

Given the marked upstream allelic heterogeneity observed across *HNF1B*-associated disease, we next asked whether cystogenesis resulting from *Hnf1b* loss remains susceptible to modulation of downstream pathways shared with other cystic kidney diseases. Pharmacologic inhibition of CFTR-mediated chloride secretion, vasopressin receptor antagonism, and systemic AMPK activation significantly attenuated cystogenesis in HNF1B-deficient kidneys. These findings provide proof-of-concept that cyst growth can remain pharmacologically modifiable despite complete *Hnf1b* loss.

Nevertheless, the effects observed in the current model were overall modest and did not translate into measurable improvement of serum creatinine or BUN at the examined early timepoint. One possible explanation is the aggressive phenotype and limited survival of the neonatal *Hnf1b* KO model, which restricts therapeutic exposure to only a few postnatal days and may prevent structural improvements from translating into detectable functional benefit. This interpretation is supported by the more pronounced effect observed with continuous metformin administration in drinking water compared with injection-based delivery.

Additional biological factors may also limit responsiveness to ADPKD-directed therapies. Recent studies in HNF1B-deficient *Xenopus* models demonstrated dysregulation of ciliopathy-associated pathways, including altered expression of genes such as *GLIS2*, *NPHP1* and *NPHP4*, whereas previously described *PKD*-associated transcriptional targets were less prominently affected[7–9,15]. Together, these findings suggest that *HNF1B*-associated cystic disease likely extends beyond classical *PKD* signaling alone and may involve broader defects in epithelial differentiation and ciliopathy-related pathways. Such complexity may explain the only partial therapeutic response observed with single-pathway interventions in the current study. In contrast, neither NMDA receptor activation nor inhibition altered cyst burden, providing no evidence for modulation of cystogenesis through the NMDA receptor axis under the conditions tested[14].

Several technical limitations should also be considered. Neonatal injections are technically challenging and may result in variable bioavailability and inconsistent renal drug exposure. In addition, the kidney-specific homozygous *Hnf1b* KO represents a severe model of HNF1B deficiency and does not fully recapitulate the heterozygous state underlying human *HNF1B* disease. The findings should therefore be interpreted as proof-of-concept rather than direct evidence of therapeutic efficacy in human *HNF1B*-associated disease. Future studies may therefore benefit from prolonged treatment paradigms, inducible or milder disease models, combinatorial therapeutic approaches, and kidney-targeted delivery systems such as nanoparticle-based strategies.

Collectively, these findings show that despite allelic heterogeneity, cystogenesis in HNF1B-deficient kidneys remains responsive to modulation of selected pathways. To our knowledge, this study provides the first evidence that pharmacologic modulation of established cystogenic pathways can reduce cyst burden in HNF1B-deficient kidneys. In parallel, our human genotype-phenotype analyses support partial allele-specific effects, with pLOF variants more frequently associated with multisystem RCAD phenotypes and missense variants showing relative enrichment for isolated diabetic presentations. At the same time, extensive allele-level phenotypic overlap emphasizes that genotype alone does not account for the variable expressivity of *HNF1B*-associated disease.

METHODS

Human *HNF1B* variant curation

Intragenic *HNF1B* variants classified as pathogenic or likely pathogenic (P/LP) in ClinVar or as disease-causing (DM) in HGMD Professional were collected. HGMD-derived variants were cross-referenced against current ClinVar classifications, and variants with benign or likely benign ClinVar classifications were excluded. ClinVar variants classified solely as variants of uncertain significance were not included. Variant nomenclature was standardized to the *HNF1B* reference transcript NM_000458.4 and protein NP_000449.1. Large genomic deletions involving the 17q12 locus were excluded to specifically assess intragenic *HNF1B* allelic heterogeneity. Synonymous variants and in-frame insertions/deletions were excluded from the comparative analyses. Variants were categorized according to predicted molecular consequence. Missense variants were analyzed separately from predicted loss-of-function (pLOF) variants, which included nonsense, frameshift, canonical splice-site, non-canonical splice-site, and start-loss variants. Distinct nucleotide changes were retained as separate alleles even when they resulted in the same predicted protein-level consequence. The final dataset comprised 329 unique intragenic alleles, including 203 pLOF and 126 missense variants (**Table S1**).

Genotype–phenotype analysis

Reported phenotypes were grouped into predefined categories including kidney-only, diabetes-only and RCAD. For consistency with the predefined curation scheme, entries reported as *HNF1B*-related disease or *HNF1B*-related disorder without further phenotypic specification were assigned to the RCAD category, reflecting the multisystem disease

spectrum often encompassed by nonspecific diagnostic labels. Because this classification may introduce ambiguity, a sensitivity analysis was additionally performed excluding alleles for which RCAD classification was based solely on such nonspecific annotations. Because the analysis was performed at the allele level rather than the patient level, individual variants contribute to multiple phenotype categories when different clinical presentations had been reported for the same allele. Curated variants were subsequently subjected to phenotype enrichment, overlap, and domain-distribution analyses. Statistical comparisons between missense and pLOF variants were performed using two-sided Fisher's exact tests. Domain-specific analyses were restricted to missense variants and mapped onto the HNF1B protein sequence according to UniProt annotation (P35680).

AlphaMissense analysis

AlphaMissense pathogenicity scores were obtained for HNF1B (UniProt P35680) and matched to the 126 missense alleles included in the final genotype–phenotype analysis. Because phenotype categories were non-mutually exclusive, AlphaMissense scores were compared separately between alleles with and without RCAD, kidney-only, or diabetes-only annotations using two-sided Mann–Whitney U tests. P values were adjusted for the three phenotype comparisons using the Holm method. For exploratory domain-adjusted analysis, the POU-specific and homeodomain regions were grouped as DNA-binding domains. Association with RCAD was further assessed by logistic regression including AlphaMissense score and DNA-binding-domain localization as predictors.

Animal studies

The Institutional Animal Care and Use Committee at Boston Children´s Hospital reviewed and approved the experimental protocols (#00001522). Mice were housed and handled according to the Guidelines for the Care and Use of Laboratory Animals with unlimited access to water and rodent chow, a light period of 12 hours per day, pathogen-free conditions, the use of analgesics and refined handling techniques to reduce pain and distress.

Mouse breeding and genotyping

Knockout (KO) mice used for this study were obtained from Dr. Peter Igarashi and previously described: KspCre+; Hnf1b$^{flox/flox}$[8,16]. Genotyping was performed according to the published protocols.

Drug treatment

The following substances were injected in the indicated quantities and time points: CFTRinh172 was administered starting at P2 (+/- 24 hours; 5 mg/kg body weight) daily by intraperitoneal (i. p.) injection diluted in 2% dimethyl sulfoxide (DMSO; **Fig. S2A**)[10]. Postnatal mice (P1 or P2) received conivaptan (0.5 mg/kg body weight) daily by retroorbital intravenous (i. v.) injection diluted in 5% dextrose solution (**Fig. S2B)**. Metformin was diluted in saline and i. p. injected (P3; 150 mg/kg body weight) daily (**Fig. S2A)**[17,18]. Additionally, the influence of early intervention on cyst development was tested by giving metformin to the pregnant dams at E10.5 and nursing mothers in the perinatal

period through drinking water (2 mg/ml)[13]. The anticipated dose would be approximately 350 mg/kg/day, although individual water consumption was not recorded[19]. Postnatal mice (P2 or P3) received AZ505 (single dose of 5 mg/kg body weight) by i. p. injection diluted in 10% DMSO solution (**Fig. S2A)**[11]. NMDA was administered by i.p. injection (P3 or P4; single dose of 7.5 mg/kg body weight; **Fig. S2A)**[20]. MK-801 was diluted in saline containing 0.05% DMSO and i.p injected (P3 or P4; single dose of 1 mg/kg body weight; **Fig. S2A**). KO mice were used for drug testing. Untreated KO mice were used as controls. Animals were randomly assigned to control and treatment groups. Both male and female mice were included in the study. Injected mice were euthanized by decapitation without prior anesthesia at P9 (±24 hours), in accordance with the institutionally approved animal protocol and applicable animal welfare guidelines, followed by cardiac puncture for blood collection, when applicable, and tissue dissection, as previous survival studies had shown an approximate survival of 75% for KO pups at P9. Heterozygous and wildtype litter mates were injected in order to assess for any adverse effects or toxicity. No unexpected adverse events were observed during the course of the study. Expected effects such as transient weight loss or mild discomfort following surgical procedures were managed according to institutional animal welfare guidelines. Inclusion and exclusion criteria were defined a priori. Animals were excluded from analysis if they showed signs of unrelated illness, died before the defined experimental endpoint, or if tissue samples were damaged or not of sufficient quality for histological or molecular analysis. All animals and data points meeting the inclusion criteria were included in the analysis. No animals or data points were excluded post hoc. To minimize potential confounding factors, animals from different groups were housed in the same rack under identical conditions.

Drug administration

Tested substances were loaded into a 100 µL Nanofil syringe equipped with a 33-gauge needle and set up with a syringe pump. I. p. injections were performed as previously described[21]. For retroorbital i. v. injections pups were cryo-anesthetized on ice for 3 to 4 minutes until a bluish body color appeared, signaling adequate anesthesia. The needle was inserted about one-third of the needle's length at a 30-45° angle into the venous sinus at the nasal position of the eye. After injection, the needle was held in place for 3 seconds before carefully removing it. Pups were placed on a 37°C heating pad to regain mobility and normal coloration.

Blood analysis

Following euthanasia, 100 µl of blood was drawn by cardiac puncture. Blood samples were collected in lithium heparin tubes and directly analyzed by the Vetscan VS2 Chemistry Analyzer using Comprehensive Diagnostic Profile rotors. Due to the limited blood volume in small and young animals, serum collection for renal function analysis was not possible in all cases. Consequently, group sizes differ between histological and biochemical assessments.

Histological studies and imaging

Kidneys were sectioned in the coronal plain, fixed in 4% paraformaldehyde over 24 hours and embedded in paraffin. 5 µm thick sections were stained with Periodic acid–Schiff (PAS) according to standard protocols. For whole section imaging, samples were

scanned using a high-resolution digital slide scanner (SLIDEVIEW VS200, Olympus, Tokyo, Japan) at 10x magnification and acquired images were processed with the analysis software Olympus OlyVIA 3.2.1.

Quantification of cystic severity

Cystic index was analyzed by ImageJ using PAS-stained images of the coronal section of the kidney as described before[22]. In short, after removal of non-cystic structures, the cystic index was calculated as the cystic area divided by the total area of the imaged kidney. This quantification was done analyzing at least one section of each kidney half. Two researchers independently performed the quantification and analysis. Cystic severity was measured by 2 kidney weight (2KW) / body weight (BW) and cystic index. Blinding was not feasible during outcome assessment; however, data analysis was conducted using coded samples to reduce bias.

Statistics

For mouse phenotype analysis, data are presented as mean ± standard deviation (SD). For cystic index, which showed heterogeneity of variance between groups, overall differences were assessed using Welch's one-way ANOVA, followed by prespecified two-sided Welch's t-tests comparing each treatment group with untreated KO controls. For comparisons of cystic index, mean differences versus untreated KO controls with 95% confidence intervals were additionally calculated. P values were adjusted for multiple comparisons using the Holm method. For 2KW/BW, BUN and creatinine, ordinary one-way ANOVA followed by Dunnett's multiple comparisons test versus untreated KO

controls was used. A two-sided p value <0.05 was considered statistically significant. OpenAI ChatGPT (GPT-5.6 Sol) was used to assist with statistical coding and data visualization. All analyses and outputs were independently reviewed and verified against the underlying data by the authors before inclusion in the manuscript.

REFERENCES

1. Kolvenbach, C. M., Shril, S. & Hildebrandt, F. The genetics and pathogenesis of CAKUT. *Nat Rev Nephrol* **19**, 709–720 (2023).
2. Clissold, R. L., Hamilton, A. J., Hattersley, A. T., Ellard, S. & Bingham, C. HNF1B-associated renal and extra-renal disease—an expanding clinical spectrum. *Nat Rev Nephrol* **11**, 102–112 (2015).
3. Ferrè, S. & Igarashi, P. New insights into the role of HNF-1β in kidney (patho)physiology. *Pediatr Nephrol* **34**, 1325–1335 (2019).
4. Gambella, A. *et al.* The Landscape of HNF1B Deficiency: A Syndrome Not Yet Fully Explored. *Cells* **12**, 307 (2023).
5. Buffin-Meyer, B. *et al.* Renal and Extrarenal Phenotypes in Patients With HNF1B Variants and Chromosome 17q12 Microdeletions. *Kidney Int Rep* **9**, 2514–2526 (2024).
6. Cao, W., Chen, Y., Wang, Y. & Xiong, J. Genotype-phenotype correlations in HNF1B-associated disease: a systematic review. *BMC Nephrol* https://doi.org/10.1186/s12882-026-05389-9 (2026) doi:10.1186/s12882-026-05389-9.
7. Shao, A., Chan, S. C. & Igarashi, P. Role of transcription factor hepatocyte nuclear factor-1β in polycystic kidney disease. *Cell Signal* **71**, 109568 (2020).
8. Gresh, L. *et al.* A transcriptional network in polycystic kidney disease. *EMBO J* **23**, 1657–1668 (2004).
9. Bergmann, C. *et al.* Mutations in Multiple PKD Genes May Explain Early and Severe Polycystic Kidney Disease. *J Am Soc Nephrol* **22**, 2047–2056 (2011).

10. Yang, B., Sonawane, N. D., Zhao, D., Somlo, S. & Verkman, A. S. Small-molecule CFTR inhibitors slow cyst growth in polycystic kidney disease. *J Am Soc Nephrol* **19**, 1300–1310 (2008).
11. Li, L. X. *et al.* Lysine methyltransferase SMYD2 promotes cyst growth in autosomal dominant polycystic kidney disease. *J Clin Invest* **127**, 2751–2764 (2017).
12. Zhou, J. X. & Torres, V. E. Drug repurposing in autosomal dominant polycystic kidney disease. *Kidney International* **103**, 859–871 (2023).
13. Pastor-Soler, N. M. *et al.* Metformin improves relevant disease parameters in an autosomal dominant polycystic kidney disease mouse model. *Am J Physiol Renal Physiol* **322**, F27–F41 (2022).
14. Bantounas, I. *et al.* Human pluripotent stem cell-derived kidney organoids reveal tubular epithelial pathobiology of heterozygous HNF1B-associated dysplastic kidney malformations. *Stem Cell Reports* **19**, 859–876 (2024).
15. Grand, K. *et al.* HNF1B Alters an Evolutionarily Conserved Nephrogenic Program of Target Genes. *J Am Soc Nephrol* **34**, 412–432 (2023).
16. Coffinier, C. *et al.* Bile system morphogenesis defects and liver dysfunction upon targeted deletion of HNF1beta. *Development* **129**, 1829–1838 (2002).
17. Zhu, Y., Fang, Y., Medina, D., Bartke, A. & Yuan, R. Metformin treatment of juvenile mice alters aging-related developmental and metabolic phenotypes. *Mech Ageing Dev* **201**, 111597 (2022).
18. Vieira, H. R. *et al.* Neonatal metformin short exposure inhibits male reproductive dysfunction caused by a high-fat diet in adult rats. *Toxicol Appl Pharmacol* **429**, 115712 (2021).

19. DiTacchio, K. A., Heinemann, S. F. & Dziewczapolski, G. Metformin treatment alters memory function in a mouse model of Alzheimer's disease. *J Alzheimers Dis* **44**, 43–48 (2015).
20. Adil, K. J. *et al.* Behavioral Deficits in Adolescent Mice after Sub-Chronic Administration of NMDA during Early Stage of Postnatal Development. *Biomol Ther (Seoul)* **30**, 320–327 (2022).
21. Pocratsky, A. M. & Sleigh, J. N. Intraperitoneal Injection of Neonatal Mice. *Bio Protoc* **13**, e4826 (2023).
22. Song, C. J. *et al.* A Comprehensive Immune Cell Atlas of Cystic Kidney Disease Reveals the Involvement of Adaptive Immune Cells in Injury-Mediated Cyst Progression in Mice. *J Am Soc Nephrol* **33**, 747–768 (2022).

ACKNOWLEDGEMENTS

We thank Dr. Igarashi for sharing his *Hnf1b* mouse model. We thank all participating collaborators for their contribution.

AUTHOR'S CONTRIBUTION

Conceptualization: C.M.K., S.S., F.H. Data curation: C.M.K., K.S., E.Z., S.H., I.E., G.K., K.L. Formal analysis: C.M.K., K.S., E.Z., S.H., S.S., F.H. Investigation: C.M.K., K.S., E.Z., S.H., S.S., F.H. Methodology: C.M.K., K.S., S.S., F.H. Project administration: S.S., F.H. Resources: F.H. Supervision: S.S., F.H. Visualization: C.M.K., K.S. Writing – original draft: C.M.K. Writing – review & editing: All authors.

DATA AVAILABILITY

All data generated or analyzed during this study are included within the manuscript and its Supplementary Information files.

COMPETING INTERESTS

The authors declare no competing interests.

FUNDING

C.M.K. and K.L. are supported by grants from the German Research Foundation (C.M.K.: 499462148 and Rückkehrstipendium KO 6579/ /3-1; K.L.: 461126211). C.M.K. is additionally supported by the Else Kröner-Fresenius-Foundation. K.S. is supported by the JSPS Overseas Research Fellowship (202260295). F. H. is the William E. Harmon

Professor of Pediatrics at Harvard Medical School. This research was supported by grants from the National Institutes of Health (NIH) to F.H. (DK076683) and by the Begg Family Foundation.

FIGURE LEGENDS

Figure 1. Overview of *HNF1B* allele curation and genotype-phenotype analysis.

A total of 329 pathogenic and likely pathogenic intragenic *HNF1B* alleles were curated from ClinVar and HGMD and classified as missense or pLOF variants. pLOF variants included nonsense, frameshift, canonical and non-canonical splice-site, and start-loss alleles. Phenotypes were categorized as kidney-only, diabetes-only or RCAD. Allele-level phenotype enrichment and domain-specific distribution analyses were subsequently performed.

Alt text: Flow diagram summarizing the curation of 329 pathogenic or likely pathogenic intragenic *HNF1B* alleles, their classification as missense or pLOF variants, phenotype categorization, and subsequent genotype–phenotype analyses.

Figure 2. Phenotypic distribution and allelic heterogeneity of curated *HNF1B* variants.

(A) UpSet plot showing the overlap of reported phenotype categories among curated intragenic *HNF1B* alleles. Dots indicate the phenotype category or combination of categories represented by each intersection; bars show the corresponding number of alleles. The substantial overlap between phenotype categories illustrates marked pleiotropy of individual *HNF1B* alleles.

(B) Comparison of phenotype reports between pLOF and missense alleles. RCAD phenotypes were significantly more frequent among pLOF alleles, whereas diabetes-only phenotypes were enriched among missense alleles. No significant difference was

observed for kidney-only phenotypes. Statistical comparisons were performed using two-sided Fisher's exact tests.

(C) Distribution of variant classes within each phenotype category or phenotype combination. Bars show the relative proportion of missense and pLOF alleles within each group. Percentages are allele-based and do not represent patient frequencies. Together, these analyses demonstrate variant-class-associated differences in phenotypic distribution despite substantial overlap between individual alleles.

Alt text: Multi-panel figure showing substantial overlap of kidney-only, diabetes-only and RCAD phenotypes among *HNF1B* alleles. pLOF variants are more frequently associated with RCAD, whereas missense variants are enriched for diabetes-only presentations.

Figure 3. Distribution of missense HNF1B alleles across the protein and domain sequence.

(A) Lollipop plot illustrating the localization of 126 curated missense variants along the full-length HNF1B protein. Functional domains are shown according to UniProt annotation (P35680), including the N-terminal dimerization domain, POU-specific DNA-binding domain, homeodomain DNA-binding motif, and C-terminal transactivation domain. Each lollipop represents one distinct missense allele, with colors indicating reported kidney-only, diabetes-only and RCAD phenotypes; multi-colored heads indicate alleles associated with multiple phenotype categories. Missense alleles were distributed throughout the protein without strong domain-specific segregation, although RCAD-associated variants showed a modest tendency to localize within the DNA-binding regions.

(B) AlphaMissense scores according to reported phenotype associations. Because phenotype categories were non-mutually exclusive, alleles associated with each phenotype were compared with alleles without the respective annotation. RCAD-associated alleles showed significantly higher AlphaMissense scores (Holm-adjusted P=0.026), whereas no significant differences were observed for kidney-only or diabetes-only phenotypes. Each point represents one allele; box plots indicate the median and interquartile range.

Alt text: Multi-panel figure showing the distribution of 126 missense *HNF1B* alleles across the HNF1B protein and their AlphaMissense scores. Variants are distributed throughout the protein without strong domain-specific phenotypic segregation; RCAD-associated variants have higher AlphaMissense scores.

Figure 4. Treatment approaches with repurposed drug candidates from ADPKD and NMDA signaling pathways.

(A) Schematic illustration of the key mechanisms of ADPKD pathogenesis and dysregulated pathways targeted by potential drug candidates (red rectangles). Conivaptan, targeting vasopressin 2 receptor (V2R), metformin, targeting AMP-activated protein kinase (AMPK) and AZ505, altering nuclear factor-κB (NF-kB) dependent epithelial cell proliferation. CFTRinh172 inhibits chloride-driven fluid secretion.

cAMP, cyclic adenosine monophosphate; CFTR, cystic fibrosis transmembrane conductance regulator; Gs, G protein alpha subunit group S; mTOR, mammalian target of rapamycin; PKA, protein kinase A; SMYD2, SET and MYND Domain Containing 2; tmAC, transmembrane adenylyl cyclases. Adapted from Zhou et al.[12]

(B) Schematic illustration of NMDA signaling mechanisms targeted by potential drug candidates (red rectangles) based on previously reported alterations in glutamatergic signaling-related genes in HNF1B-deficient epithelia. MK-801, a non-competitive NMDA receptor (NMDAR) antagonist, inhibits ion conduction. NMDA is an agonist molecule and binds selectively to the glutamate receptor. Potential interaction between HNF1B and glutamatergic signaling through iGluR kainate type subunit 3 (GRIK3) is outlined.
Created in BioRender. Saida, K. (2025) https://BioRender.com/3288pix and https://BioRender.com/871jiew
Alt text: Two schematic pathway diagrams illustrating candidate pharmacologic targets in ADPKD-associated cystogenic pathways and glutamatergic signaling. The diagrams indicate the proposed targets of conivaptan, metformin, AZ505, CFTRinh172, MK-801 and NMDA and their potential relationship to *HNF1B*-associated kidney disease.

Figure 5. Pharmacologic modulation of cystogenesis in *Hnf1b* KO mice

(A) Cystic indices of untreated or candidate drugs treated KO mice are depicted. Each data point presents the mean of cystic index per animal. A significant difference was observed for KO pups treated with CFTRinh172 (n=5), conivaptan (n=5) and metformin through drinking water (n=3; adjusted $p<0.05$). No significant difference was noted for any of the other applied candidate drugs. Untreated KO mice: n=14; metformin i.p. n=4; AZ505: n=4; MK-801: n=6; NMDA: n=5. *$p<0.05$; **$p<0.01$

(B) The ratio of 2KW/BW is shown. A significant increase was noted for KO pups treated with CFTRinh172. No significant difference was observed for any of the other tested drug candidates.

(C) BUN levels in KO mice treated with drug candidates. No significant difference was observed between treated or untreated mice. Untreated KO mice: n=7; CFTRinh172: n=4; conivaptan: n=5; metformin through drinking water: n=3; metformin i.p. n=3; AZ505: n=4; MK-801: n=7; NMDA: n=5.

(D) Creatinine levels in KO mice treated with ADPKD and NMDA derived drug candidates or untreated controls. No significant difference was observed between treated or untreated mice.

(E-F) Representative section images of cystic kidneys from KO mice treated with or without CFTRinh172 at P9. Scale bar: 2 mm

Alt text: Multi-panel figure comparing cystic kidney disease severity and renal parameters in untreated and drug-treated *Hnf1b* KO mice. CFTRinh172, conivaptan and oral metformin reduce cystic burden, whereas the other tested interventions show no significant effect; representative kidney sections illustrate reduced cystic changes after CFTRinh172 treatment.

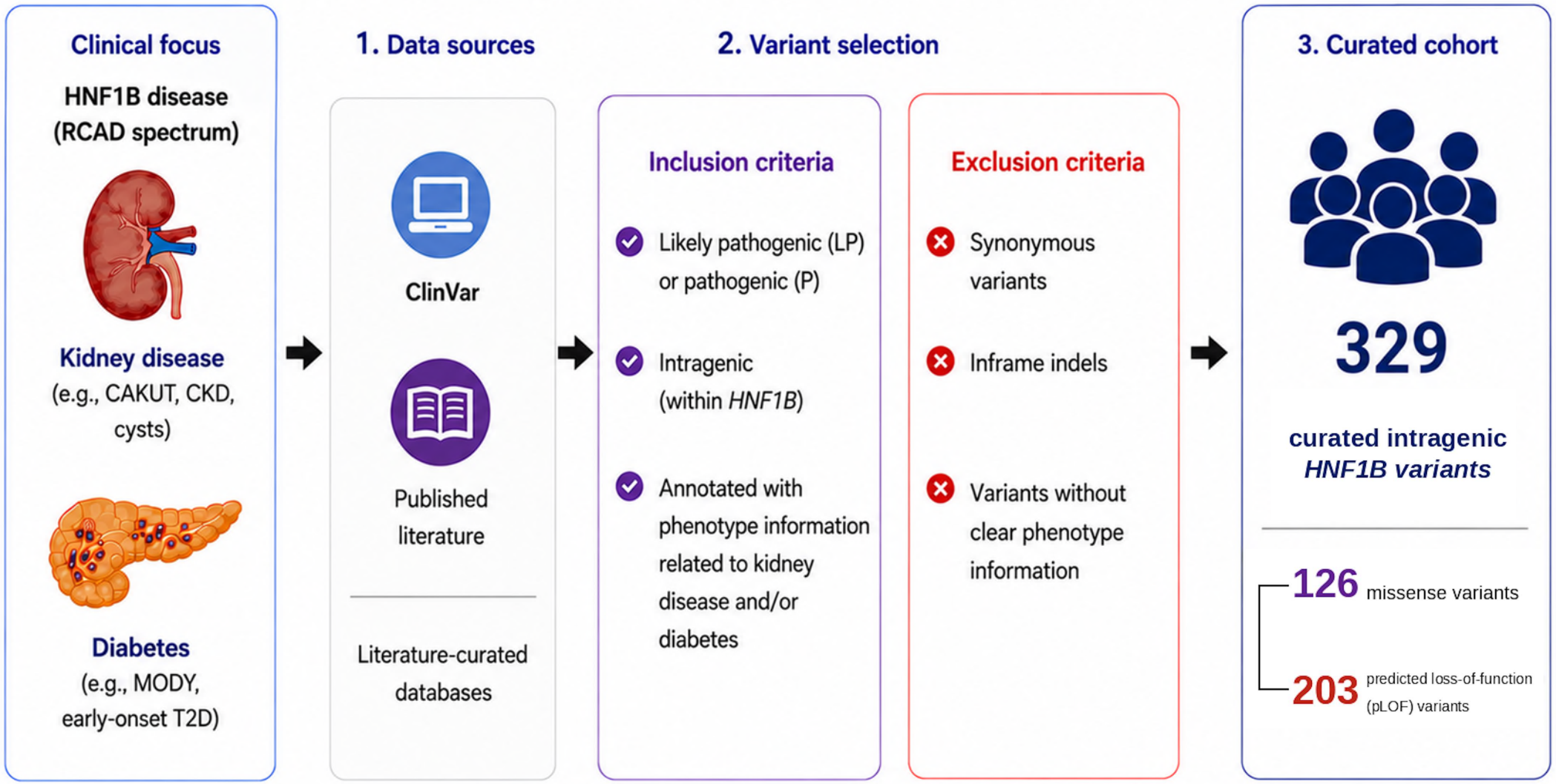

Clinical focus
HNF1B disease
(RCAD spectrum)
Kidney disease
(e.g., CAKUT, CKD, cysts)
Diabetes
(e.g., MODY, early-onset T2D)
1. Data sources
ClinVar
Published literature
Literature-curated databases
2. Variant selection
Inclusion criteria
Likely pathogenic (LP) or pathogenic (P)
Intragenic (within HNF1B)
Annotated with phenotype information related to kidney disease and/or diabetes
Exclusion criteria
Synonymous variants
Inframe indels
Variants without clear phenotype information
3. Curated cohort
329
curated intragenic HNF1B variants
126 missense variants
203 predicted loss-of-function (pLOF) variants

Figure 1

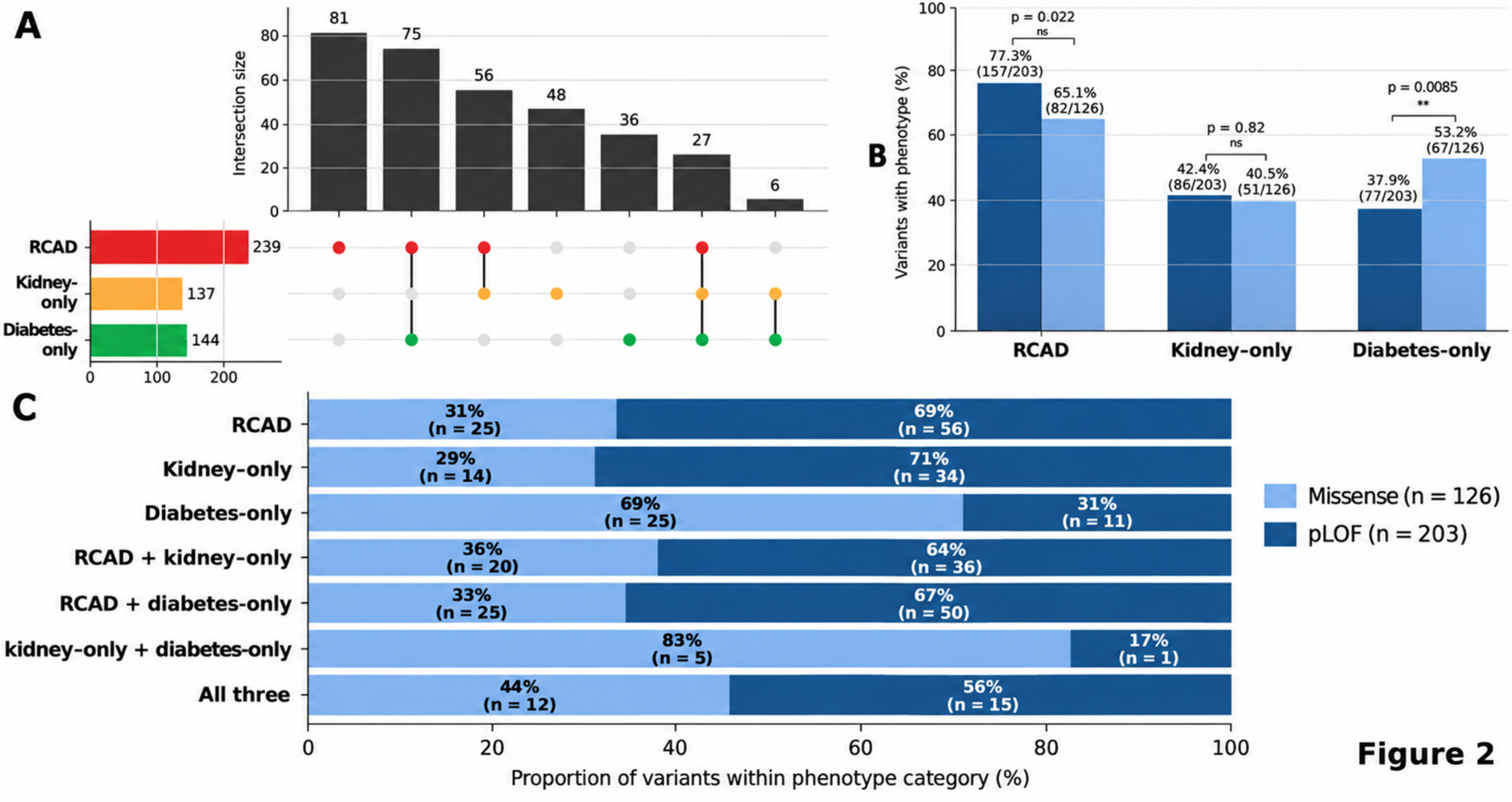
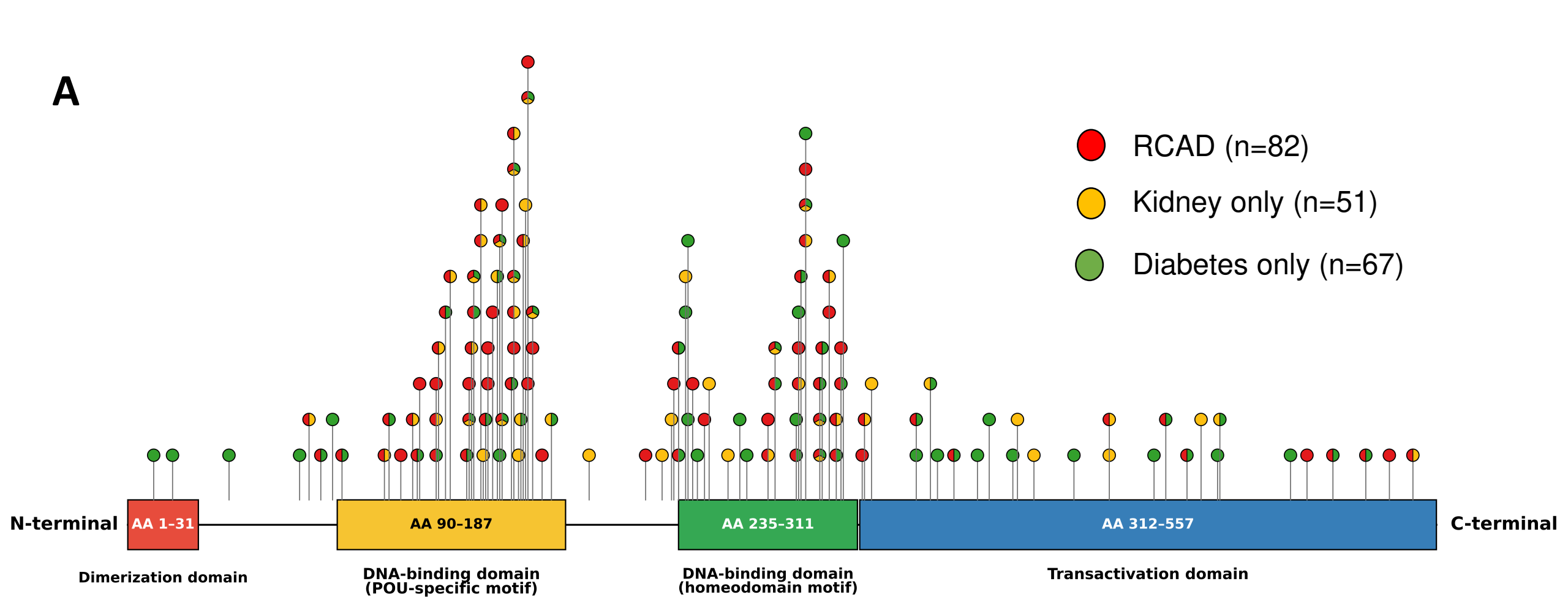

A
Intersection size
81
75
56
48
36
27
6
RCAD
Kidney-only
Diabetes-only
239
137
144
B
Variants with phenotype (%)
p = 0.022
ns
77.3% (157/203)
65.1% (82/126)
p = 0.82
ns
42.4% (86/203)
40.5% (51/126)
p = 0.0085
**
37.9% (77/203)
53.2% (67/126)
RCAD
Kidney-only
Diabetes-only
C
RCAD
31% (n = 25)
69% (n = 56)
Kidney-only
29% (n = 14)
71% (n = 34)
Diabetes-only
69% (n = 25)
31% (n = 11)
RCAD + kidney-only
36% (n = 20)
64% (n = 36)
RCAD + diabetes-only
33% (n = 25)
67% (n = 50)
kidney-only + diabetes-only
83% (n = 5)
17% (n = 1)
All three
44% (n = 12)
56% (n = 15)
Missense (n = 126)
pLOF (n = 203)
Proportion of variants within phenotype category (%)

Figure 2


A
RCAD (n=82)
Kidney only (n=51)
Diabetes only (n=67)
N-terminal
AA 1–31
AA 90–187
AA 235–311
AA 312–557
C-terminal
Dimerization domain
DNA-binding domain
(POU-specific motif)
DNA-binding domain
(homeodomain motif)
Transactivation domain

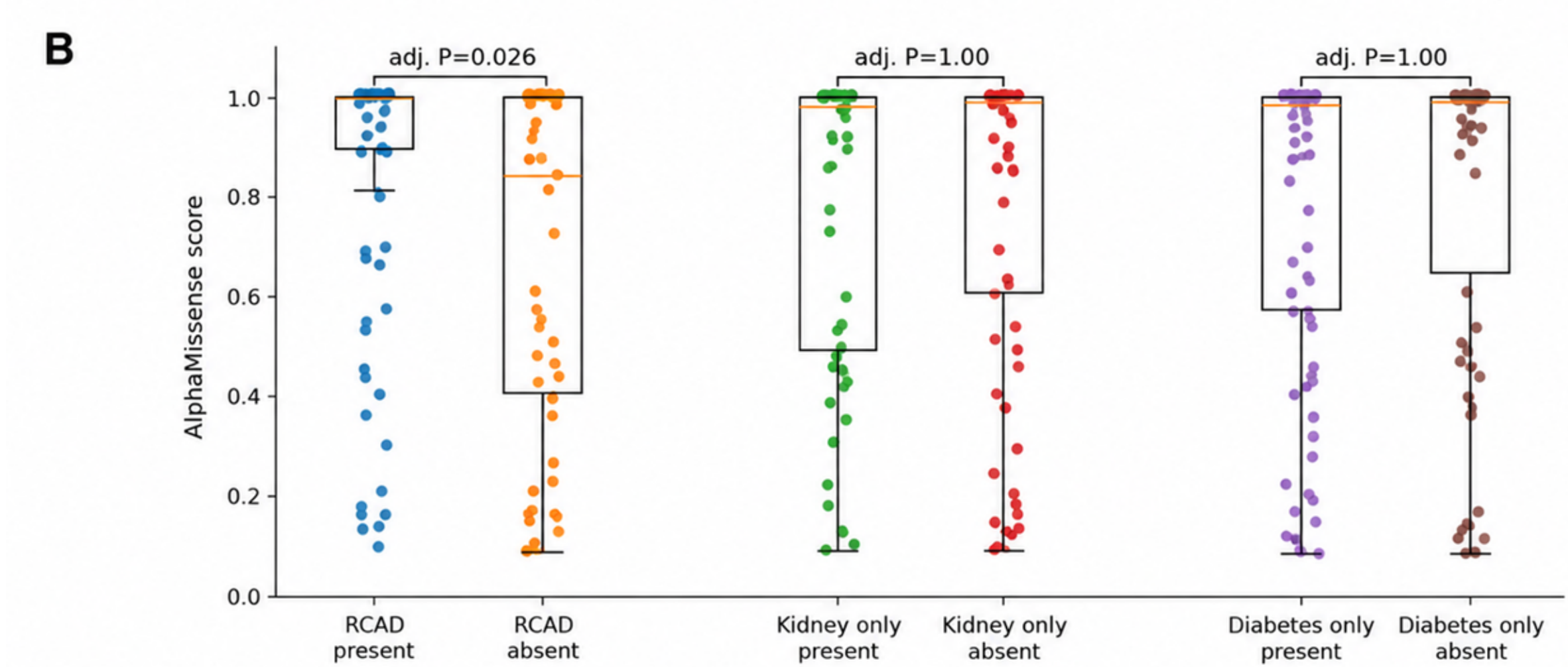

B
adj. P=0.026
adj. P=1.00
adj. P=1.00
AlphaMissense score
1.0
0.8
0.6
0.4
0.2
0.0
RCAD present
RCAD absent
Kidney only present
Kidney only absent
Diabetes only present
Diabetes only absent

Figure 3

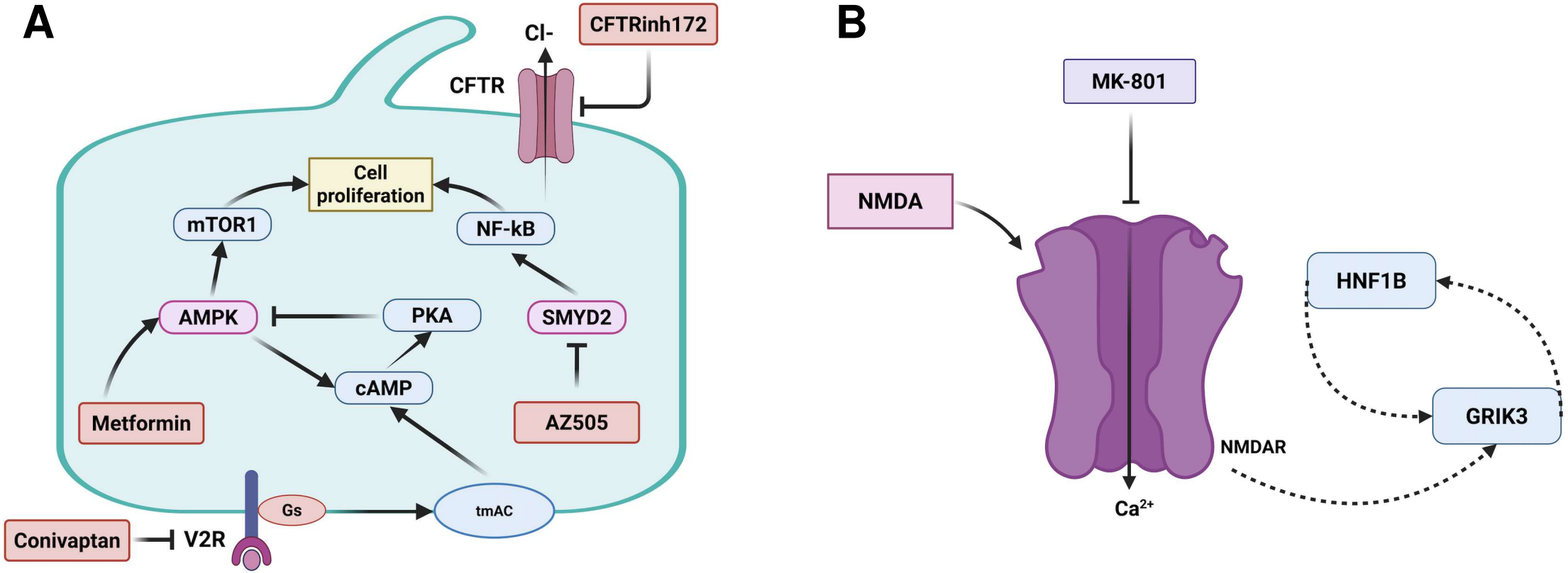

A
Cl-
CFTRinh172
CFTR
Cell proliferation
mTOR1
NF-kB
AMPK
PKA
SMYD2
cAMP
Metformin
AZ505
Gs
tmAC
Conivaptan
V2R
B
MK-801
NMDA
HNF1B
GRIK3
NMDAR
Ca2+

Figure 4

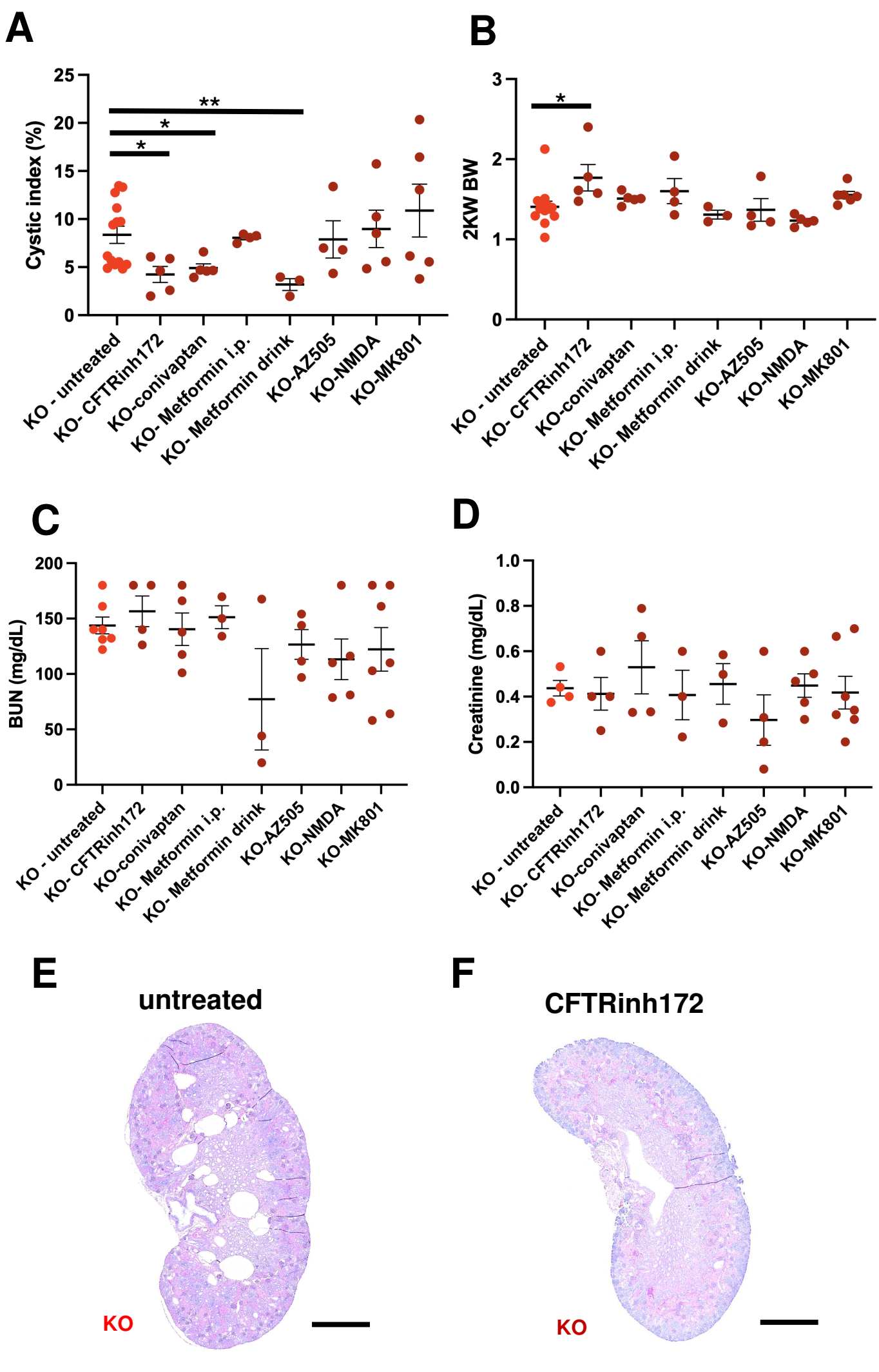

A
Cystic index (%)
25
20
15
10
5
0
**
*
*
KO - untreated
KO- CFTRinh172
KO-conivaptan
KO- Metformin i.p.
KO- Metformin drink
KO-AZ505
KO-NMDA
KO-MK801
B
2KW BW
3
2
1
0
*
KO - untreated
KO- CFTRinh172
KO-conivaptan
KO- Metformin i.p.
KO- Metformin drink
KO-AZ505
KO-NMDA
KO-MK801
C
BUN (mg/dL)
200
150
100
50
0
KO - untreated
KO- CFTRinh172
KO-conivaptan
KO- Metformin i.p.
KO- Metformin drink
KO-AZ505
KO-NMDA
KO-MK801
D
Creatinine (mg/dL)
1.0
0.8
0.6
0.4
0.2
0.0
KO - untreated
KO- CFTRinh172
KO-conivaptan
KO- Metformin i.p.
KO- Metformin drink
KO-AZ505
KO-NMDA
KO-MK801
E
untreated
KO
F
CFTRinh172
KO

Figure 5

Supplementary Files

This is a list of supplementary files associated with this preprint. Click to download.

- 1Supplement.docx
- TableS1.xlsx
- FigureS1.pptx
- FigureS2.pptx